PB82-154907

Broadening of the RF Power-Density Window for Calcium-Ion Efflux from Brain Tissue

(U.S.) Health Effects Research Lab.
Research Triangle Park, NC

16 Mar 81

U.S. Department of Commerce
National Technical Information Service
NTIS

TECHNICAL REPORT DATA
(Please read Instructions on the reverse before completing)

MS-81-013

1. REPORT NO.	2.	3.
EPA-600/J-81-514	JOURNAL ARTICLE	PB82-154907

4. TITLE AND SUBTITLE
Broadening of the RF Power-Density Window for Calcium-Ion Efflux from Brain Tissue

5. REPORT DATE
January 1982

6. PERFORMING ORGANIZATION CODE
025110

7. AUTHOR(S)
William T. Joines, Carl F. Blackman, and Mark A. Hollis

8. PERFORMING ORGANIZATION REPORT NO.

9. PERFORMING ORGANIZATION NAME AND ADDRESS
Experimental Biology Division
Health Effects Research Laboratory
US Environmental Protection Agency
Research Triangle Park, NC 27711

10. PROGRAM ELEMENT NO.

11. CONTRACT/GRANT NO.

12. SPONSORING AGENCY NAME AND ADDRESS
Office of Research and Development (RTP,NC)
Health Effects Research Laboratory
US Environmental Protection Agency
Research Triangle Park, NC 27711

13. TYPE OF REPORT AND PERIOD COVERED

14. SPONSORING AGENCY CODE
EPA-600/11

15. SUPPLEMENTARY NOTES
Published In: IEEE Transactions on Biomedical Eng. 28(8): 568-573, 1981

16. ABSTRACT

Blackman, et.al. have reported enhanced efflux of calcium ions from chicken forebrains, exposed in vitro in a 50 Ω stripline to 147 MHz radiation, modulated sinusoidally at 16 Hz. When the spacing between the sample tubes was 3.8 cm on center, enhancement occured at an incident power density of 0.83 mW/cm , but not at 0.11, 0.55, 1.11, or 1.38 mW/cm^2. When the spacing between sample tubes was reduced to 1.9 cm, significant enhanced efflux was observed at incident power densities of 0.55, 0.83, 1.11, and 1.38 mW/cm^2. This broadening of the effective power-density range is explained herein by calculations which show that the more closely spaced samples interact electrically in a way that both lowers and broadens the range of spatial variation of absorbed power density ($\mu W/cm^3$) within the sample for a given incident power density (mW/cm^2). Electrical coupling among the samples allows several different values of incident power to yield exactly the same value of power absorber at given points within the brain sample. Because the absorbed power density must be directly related to the power that interacts with the brain to enhance the efflux of calcium ions, the electromagnetic conditions for efflux enhancement in coupled and uncoupled brains are the same if the absorbed power density is the same. Ranges of absorbed power density are identified that could be effective in enhancing the efflux of calcium ions from the brain tissue.

17. KEY WORDS AND DOCUMENT ANALYSIS

a. DESCRIPTORS	b. IDENTIFIERS/OPEN ENDED TERMS	c. COSATI Field/Group

REPRODUCED BY
NATIONAL TECHNICAL
INFORMATION SERVICE
U.S. DEPARTMENT OF COMMERCE
SPRINGFIELD, VA 22161

18. DISTRIBUTION STATEMENT	19. SECURITY CLASS (This Report)	21. NO. OF PAGES
RELEASE TO PUBLIC	UNCLASSIFIED	8
	20. SECURITY CLASS (This page)	22. PRICE
	UNCLASSIFIED	

EPA-600/J-81-514
Journal Article

Broadening of the RF Power-Density Window for Calcium-Ion Efflux from Brain Tissue

WILLIAM T. JOINES, MEMBER, IEEE, CARL F. BLACKMAN, AND MARK A. HOLLIS, STUDENT MEMBER, IEEE

Abstract—Blackman *et al.* [1], [2] have reported enhanced efflux of calcium ions from chicken forebrains, exposed *in vitro* in a 50 Ω stripline to 147 MHz radiation, modulated sinusoidally at 16 Hz. When the spacing between the sample tubes was 3.8 cm on center, enhancement occurred at an incident power density of 0.83 mW/cm^2, but not at 0.11, 0.55, 1.11, or 1.38 mW/cm^2. When the spacing between sample tubes was reduced to 1.9 cm, significant enhanced efflux was observed at incident power densities of 0.55, 0.83, 1.11, and 1.38 mW/cm^2. This broadening of the effective power-density range is explained herein by calculations which show that the more closely spaced samples interact electrically in a way that both lowers and broadens the range of spatial variation of absorbed power density (μW/cm^3) within the sample for a given incident power density (mW/cm^2). Electrical coupling among the samples allows several different values of incident power to yield exactly the same value of power absorbed at given points within the brain sample. Because the absorbed power density must be directly related to the power that interacts with the brain to enhance the efflux of calcium ions, the electromagnetic conditions for efflux enhancement in coupled and uncoupled brains are the same if the absorbed power density is the same. Ranges of absorbed power density are identified that could be effective in enhancing the efflux of calcium ions from the brain tissue.

Introduction

RADIO frequency (RF) radiation, amplitude modulated at sub-ELF, has been shown to cause enhanced efflux of calcium ions from chicken forebrains exposed *in vitro* [1]. The range of incident power densities that causes this enhanced efflux is dependent on the number of samples exposed simultaneously [2]. Calculations developed in this report show that a wide range of incident power densities produces the same internal absorbed power density when the tissue samples are physically and electrically close together in the RF field. Because the absorbed power density must be directly related to the RF signal that interacts with the brain to enhance the efflux of calcium ions, this paper relies upon these calculations in explaining why electrically coupled brain samples have displayed enhanced efflux over a wider range of incident power densities than nonelectrically coupled brain samples. This analysis is applied to the results of previous experiments; therefore, a brief description of those experiments is in order.

Manuscript received February 21, 1980; revised March 16, 1981.

W. T. Joines is with the Experimental Biology Division, Health Effects Research Laboratory, U.S. Environmental Protection Agency, Research Triangle Park, NC 27711, and with the Department of Electrical Engineering, Duke University, Durham, NC 27706.

C. F. Blackman is with the Experimental Biology Division, Health Effects Research Laboratory, U.S. Environmental Protection Agency, Research Triangle Park, NC 27711.

M. A. Hollis was with the Experimental Biology Division, Health Effects Research Laboratory, U.S. Environmental Protection Agency, Research Triangle Park, NC 27711. He is now with the School of Electrical Engineering, Cornell University, Ithaca, NY 14850.

Changes in calcium-ion binding to brain tissue exposed *in vitro* to a specific incident power density (0.83 mW/cm^2) of 147 MHz radiation, amplitude modulated by a 16 Hz sine wave, has been reported by Blackman *et al.* To determine more precisely the incident power densities that are effective in producing changes in calcium ion binding, an additional series of experiments was conducted with four test tube samples and with ten test tube samples in a stripline, again using 147 MHz radiation, sinusoidally modulated at 16 Hz [2]. In the first series of experiments, all four test tubes contained chick brain halves immersed in buffer medium, while in the second series of experiments chick brain halves were located at the same four positions, but test tubes containing an equivalent amount of buffer solution were located at the six remaining positions.

In these experiments, unlike the narrow power-density window found for four samples, the ten-sample configuration resulted in a broader window of incident power densities that is effective in producing enhanced efflux of calcium ions. Mathematical developments contained in the following sections of this paper show that dipole interactions between the closely spaced samples change the distribution of absorbed power within a sample, thus changing the range of incident power densities that are effective. The goal of the theoretical analysis is to find the range of spatial distribution of absorbed power density P_a (in μW/cm^3) within a sample for each value of incident power density P_i (in mW/cm^2) impinging upon the sample, and thus to apply the results of the analysis to explain the observed results from the chick brain experiments.

Materials and Methods

Sample Dimensions and Spacing

The test tube samples are held in a Lucite rack and placed in an air-filled stripline having a characteristic impedance of 50 Ω. A cross-sectional view of the stripline, looking down on the tops of the test tubes in the direction of energy propagation, is shown in Fig. 1. The hemispherical bottom of a test tube has an inner radius $a = 0.71$ cm. A spherical volume corresponding to this radius is $(4\pi/3)a^3$ or 1.5 cm^3. Each test tube sample has approximately this volume, which is composed of a chick brain half plus buffer solution, or buffer solution alone. A chick brain half nestled at the bottom of a test tube has a mean horizontal dimension of 1 cm and a mean height of 0.81 cm. The mean height from the top of a brain half to the surface of buffer solution is 0.24 cm. Since the test tube is plastic and the diameter is 1.42 cm, the surface of the buffer solution is essentially flat across the entire diameter. The test tubes containing brain tissue in Fig. 1 are labeled (*BT*). The

0018-9294/81/0800-0568$00.75

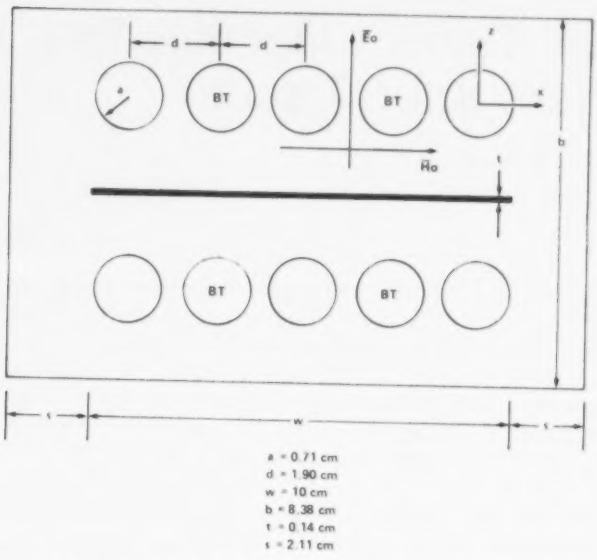

Fig. 1. Cross-sectional view of the 50 Ω stripline, looking down on the tops of test tubes in the direction of propagation. The brain-tissue samples are labeled (*BT*). The directions of the $\bar{E}$ and $\bar{H}$ fields and various dimensions are as indicated.

remaining six test tubes contain buffer solution equivalent to the volume of brain plus solution. These six test tubes are removed for all four-sample experiments. Hence, the spacing between sample centers for ten samples in the line is $d = 1.90$ cm, and for four samples the spacing is $2d = 3.80$ cm.

Electric Field Induced Inside Samples

Except for the flat-topped meniscus of the buffer solution, each sample at the bottom of a test tube is approximately spherical in shape. For analytical convenience, we assume each sample to be a sphere of radius a composed of the buffer solution alone, or the buffer solution plus brain tissue. Each sample is irradiated by a uniform plane-wave field similar to the far field of an antenna. The relative electric field intensity induced inside a single sphere [neglecting adjacent spheres as in Fig. 2(a)] of radius $a \ll \lambda$ (wavelength in air) is given by the vector equation taken from Spiegel [3] and Lin *et al.* [4].

$$\frac{\bar{E}}{E_0} = \frac{3\hat{z}}{2 + \epsilon_r^*} - j\frac{\pi}{\lambda}(y\hat{z} - z\hat{y}) \tag{1}$$

where $\hat{y}$ and $\hat{z}$ are unit vectors in the y and z directions, respectively,

$$\epsilon_r^* = \frac{\epsilon}{\epsilon_0} - j\frac{\sigma}{\omega\epsilon_0}$$

is the relative complex permittivity, σ is the sample conductivity, ω is the radian frequency, and $e^{j\omega t}$ time dependence is assumed for all fields. The first term in (1) is due to the incident uniform electric field E_0, and the second term is due to the incident uniform magnetic field $H_0 = E_0/\eta_0$ in the stripline, where $\eta_0 = 377\ \Omega$, the intrinsic impedance of free space. This expression for the electric field intensity inside a single sphere is used to calculate the time-averaged absorbed power density within the sphere.

Calculated Results

Power Absorbed in Isolated Sphere

The time-averaged incident power density P_i within the uniform field of the stripline is

$$P_i = \tfrac{1}{2} E_0^2/\eta_0 \tag{2}$$

in W/m^2 if E_0 is in V/m. At a given point inside the spherical sample, the time-averaged absorbed power density P_a is

$$P_a = \tfrac{1}{2}\sigma\bar{E}\cdot\bar{E}^* = \tfrac{1}{2}\sigma E^2 \tag{3}$$

in W/m^3 for σ in mho/m and E in V/m. The absorbed power density relative to the incident power density is obtained from the ratio of (2) and (3).

$$\frac{P_a}{P_i} = \eta_0 \sigma E^2/E_0^2 . \tag{4}$$

The ratio E^2/E_0^2 is obtained by taking the dot product of (1) and its complex conjugate, and using the relation $\omega\epsilon_0\eta_0 = 2\pi/\lambda$. The result is

$$\frac{E^2}{E_0^2} = \frac{9 - 3\eta_0\sigma y}{\left(2 + \frac{\epsilon}{\epsilon_0}\right)^2 + \left(\frac{\sigma}{\omega\epsilon_0}\right)^2} + \left(\frac{\pi}{\lambda}\right)^2 (y^2 + z^2). \tag{5}$$

For a sphere of radius $a = 0.0071$ m, at 147 MHz, where $\sigma = 0.565$ mho/m and $\epsilon/\epsilon_0 = 66$ for brain tissue [5], the variation of P_a/P_i across the sphere's diameter in the x, y, and z direction is calculated from (4) and (5) and displayed on the left in Fig. 3.

Cylindrical Limit for Close Spacing

For four samples in the stripline, the interaction between adjacent spheres (3.8 cm apart) is negligible and the diagram on the left in Fig. 3 accurately represents P_a/P_i for any of the spherical samples. Useful insight on how P_a/P_i changes for a given sphere as adjacent spheres are brought closer is obtained by examining the limiting case of spheres so close together along the x axis that they form a continuous cylinder of radius $a = 0.0071$ m as indicated in Fig. 2(b). Using methods cited earlier [3], [4], the relative electric field intensity induced inside the cylinder is expressed by the vector equation

$$\frac{\bar{E}}{E_0} = \frac{2\hat{z}}{1 + \epsilon_r^*} - j\frac{\pi}{\lambda}(y\hat{z} - z\hat{y}) \tag{6}$$

where all parameters are defined as in (1). In this case, P_a/P_i is again given by (4), and E^2/E_0^2 is obtained as the dot product of (6) and its complex conjugate as

$$\frac{E^2}{E_0^2} = \frac{4 - 2\eta_0\sigma y}{[1 + (\epsilon/\epsilon_0)]^2 + [(\sigma/\omega\epsilon_0)]^2} + \left(\frac{\pi}{\lambda}\right)^2 (y^2 + z^2) \tag{7}$$

for the cylinder along the x axis. Again taking $\sigma = 0.565$ mho/m and $\epsilon/\epsilon_0 = 66$ at 147 MHz, P_a/P_i along each axis through the cylinder is calculated and displayed on the right in Fig. 3. For a given sphere with adjacent spheres close enough to cause an

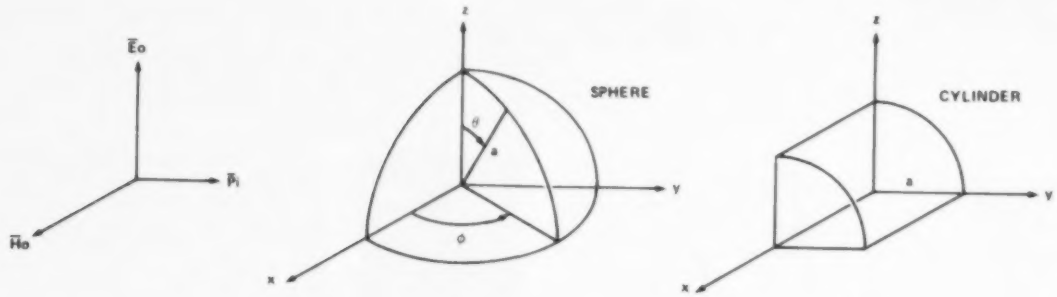

Fig. 2. (a) Single sphere of radius much smaller than the wavelength, irradiated by a uniform electromagnetic field propagating along the y axis. (b) Limiting case of spheres so close together along the x axis that they form a continuous cylinder of radius a, and irradiated as described above.

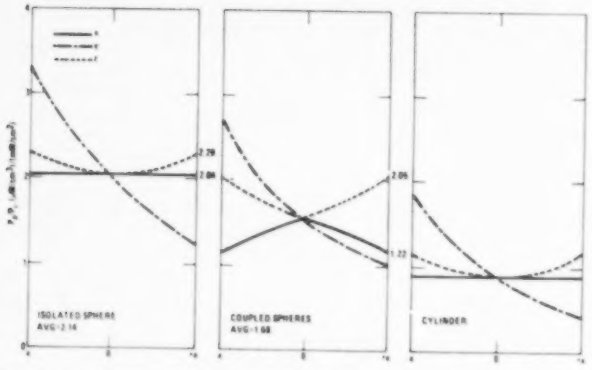

Fig. 3. Variation of P_a/P_i from $-a$ to $+a$ along the x, y, and z axes for an isolated sphere (left), a sphere with interacting adjacent spheres (center), and a continuous cylinder (right).

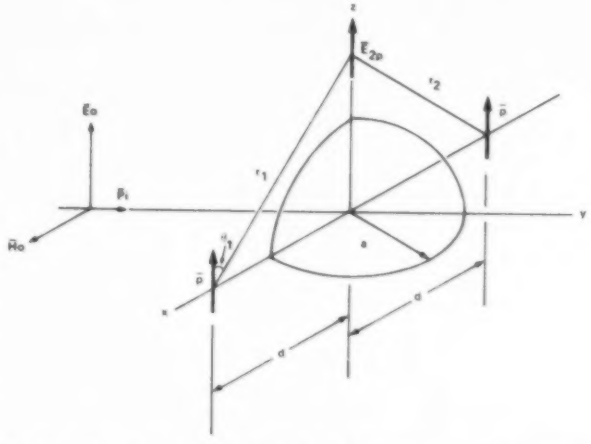

Fig. 4. Adjacent spheres are replaced by dipoles of moment $\bar{p}$ to determine the equivalent electric field applied to the central sphere.

interaction, P_a/P_i should lie between the left- and right-hand curves in Fig. 3.

Dipole Field of Adjacent Spheres

The influence of adjacent spheres on the expressions derived for absorbed power density relative to incident power density, (4) and (5), will now be determined. A sphere of complex permittivity $\epsilon^* = \epsilon - j\sigma/\omega$, placed in a uniform field E_0, alters the field in the vicinity of the sphere so that the field is no longer uniform. At all points outside the radius a, the effect of the sphere is equivalent to that of an electric dipole moment $\bar{p}$ at the center of the sphere it is replacing, of value

$$\bar{p} = 4\pi\,\epsilon_0\,a^3\left(\frac{\epsilon^* - \epsilon_0}{\epsilon^* + 2\epsilon_0}\right)\bar{E}_0. \tag{8}$$

Equation (8) follows directly from the electric flux density $\bar{D} = \epsilon^*\,\bar{E}$ within the sphere expressed as

$$\bar{D} = \epsilon_0\bar{E} + \bar{P} \tag{9}$$

or

$$\bar{P} = (\epsilon^* - \epsilon_0)\,\bar{E} \tag{10}$$

where $\bar{P}$ is the electric dipole moment per unit volume. Integrating $\bar{P}$ over the spherical volume of radius a, and using $\bar{E}$ from (1), yields $\bar{p}$ as in (8). As a check of (8), the two extreme cases of a perfect conductor ($\epsilon^* = -j\sigma/\omega$) and a perfect dielectric ($\epsilon^* = \epsilon$) are seen to yield correct values of $\bar{p}$ [6].

To determine the influence of adjacent spheres on the field applied to a given sphere, the adjacent spheres are replaced by dipoles of moment $\bar{p}$ as indicated in Fig. 4. The r_1 and θ_1 components of the electric field intensity due to the dipole at $(d, 0, 0)$ in Fig. 4 are [6]

$$E_{r_1} = \frac{2p\cos\theta_1}{4\pi\epsilon_0 r_1^3} \tag{11}$$

and

$$E_{\theta_1} = \frac{p\sin\theta_1}{4\pi\epsilon_0 r_1^3}. \tag{12}$$

Similar expressions would be written for the dipole at $(-d, 0, 0)$. When the electric field intensities contributed by the two dipoles are added together along the x, y, and z axes of Fig. 4, only the z-directed component remains. This field component for the first dipole is

$$E_z = E_{r_1}\cos\theta_1 - E_{\theta_1}\sin\theta_1. \tag{13}$$

Using (11) and (12), we have

$$E_z = \frac{p}{4\pi\epsilon_0 r_1^3}(2\cos^2\theta_1 - \sin^2\theta_1)$$

$$= \frac{p}{4\pi\epsilon_0 r_1^3}(3\cos^2\theta_1 - 1). \quad (14)$$

Adding to (14) a similar contribution from the second dipole, and using (8), we find that along the *xyz* axes of a given sphere, the electric field intensity contributed by the two adjacent dipoles is directed along $\bar{E}_0$ and has the value

$$\bar{E}_{2p} = a^3\left(\frac{\epsilon^* - \epsilon_0}{\epsilon^* + 2\epsilon_0}\right)\bar{E}_0(3\cos^2\theta_1 - 1)\left(\frac{1}{r_1^3} + \frac{1}{r_2^3}\right) \quad (15)$$

where $r_2 = r_1$ along the y and z axes, and $r_1 = 2d - r_2$ along the x axis. Hence, the new electric field applied to a sphere between adjacent spheres is

$$\bar{E}_0' = \bar{E}_0 + \bar{E}_{2p}. \quad (16)$$

The limiting values for $\bar{E}_{2p}$ can be determined from Fig. 4 by noting that for $d = 2a$ (spheres touching), $\cos^2\theta_1$ ranges from 0 to 0.25 over the volume of the center sphere. Hence, for all values of $d \geq 2a$, $\cos^2\theta_1 \leq 0.25$. Thus, E_{2p} in (15) is always negative, and E_0' is always less than E_0. Using $(E_0')^2$ from (16) in place of E_0^2 in (5), the axial values of P_a/P_i for a sphere influenced by two adjacent spheres (ten samples in the stripline) are calculated and represented by the middle curves in Fig. 3 for the dimensions given in Fig. 1.

For a more precise determination of $\bar{E}_0'$, two additional terms would be included on the right-hand side of (16). A term could be added to account for the change in E_0 at a given sphere due to the mutual interaction between the dipoles of adjacent spheres. Rather lengthy calculations based upon the solution for electrical images of point charges in conducting and dielectric spheres [7] show that the mutual interaction term would contribute less than $0.02E_0$ for the dimensions in Fig. 1; hence, this term is neglected.

A term could also be added to (16) to account for the change in E_0 at a given sphere due to the dipole-like sphere's interaction with the conducting planes of the stripline. By imaging the sphere's dipole into each plane and calculating the electric field at the site of the sphere due to its imaged dipoles, the contribution to E_0' is again less than $0.02E_0$. Hence, this term is also neglected.

Discussion

The curves for isolated and coupled spheres in Fig. 3 demonstrate that range of variation and average value of P_a/P_i over the volume is quite different for brain halves in the four-sample case (left) compared to the ten-sample case (middle). The average value of P_a/P_i is decreased from 2.14 to 1.68, and the range of variation along the x and z axes is expanded by a factor of $(2.05 - 1.22)/(2.29 - 2.04) = 3.32$ in going from isolated to coupled spheres. These differences in absorbed power for a given incident power should relate directly to the differing results obtained for the measured enhancement of calcium-ion efflux for the two cases. Recall that for isolated spheres, enhancement occurred at an incident power density of 0.83 mW/cm^2, but not at 0.11, 0.55, 1.11, or 1.38 mW/cm^2; and for coupled spheres, enhancement occurred at incident power densities of 0.55, 0.83, 1.11, and 1.38 mW/cm^2. If a given level of absorbed power density is effective in producing calcium-ion efflux, then the amount of total efflux should be directly proportional to the amount of volume and surface over which the effective power level occurs. An effective power level applied over too small a region may not produce enough calcium efflux to be measurable.

Based upon the above discussion and the results in Fig. 3, we assume as a working hypothesis that for the isolated-sphere case a specific value of P_a for a given P_i from 2.04 to 2.29 (bracketing the average value of 2.14) is effective in enhancing calcium efflux; and that for the coupled-sphere case, a specific value of P_a for a given P_i from 1.22 to 2.05 (bracketing the 1.68 average) is effective. This assures that a sizable region within and on a brain tissue sample is subjected to the same value of P_a/P_i. For these P_a/P_i ranges, the continuous range of calculated values of P_a (in μW/cm^3) within the volume caused by P_i (in mW/cm^2) values used in calcium efflux experiments [2] is shown in Fig. 5. At each test value of P_i, P_a for an isolated sphere is indicated by a leftward bar and P_a for a sphere influenced by adjacent spheres is indicated by a rightward bar. Symbols to denote positive and negative test results are also indicated.

For example, in Fig. 5 a P_i of 0.83 mW/cm^2 yielded positive test results for both isolated and interacting spheres, as indicated by the black bars. For 0.83 mW/cm^2 incident upon an isolated sphere, the P_a/P_i range of 2.04–2.29 defines a P_a range of 1.69–1.90 μW/cm^3, as denoted by the leftward bar above 0.83 in Fig. 5. In a similar manner, the rightward bar above 0.83 mW/cm^2 indicates that P_a ranges from 1.01–1.70 μW/cm^3 for a sphere with interacting neighbors, in correspondence with the P_a/P_i range of 1.22–2.05.

There are, of course, errors due to approximation and measurement that affect both P_a and P_i in Fig. 5. The "spherical" samples are flat topped at the level of the buffer solution, and the 0.08 cm thickness of plastic test tube surrounding the sample has been neglected. Since at 147 MHz the test tube wall is only 0.0004 λ thick, and has electrical properties close to those of air, the effect of the test tube wall should be negligible.

In order to obtain a closed-form solution for the induced fields within the flat-topped spherical-bottomed samples, we have modeled each test tube sample as a sphere of equal volume. We could not have obtained a closed-form solution if the samples had been modeled as cylinders. Since the actual brain tissue is located within the lower four-fifths of the total sample height (within the spherical-shaped bottom of the test tube), our calculated results should be in close agreement with the fields that are induced within the brain tissue.

By methods described elsewhere [8], we have measured the dielectric properties of the buffer solution to be relatively close to those for the chicken forebrain at 147 MHz. This agreement, we believe, is close enough to allow the sample to be treated in theoretical terms as an electrically homogeneous object in the stripline.

Due to errors in measuring P_i in the stripline, the values on the abscissa in Fig. 5 are accurate to within ±3.5 percent. The

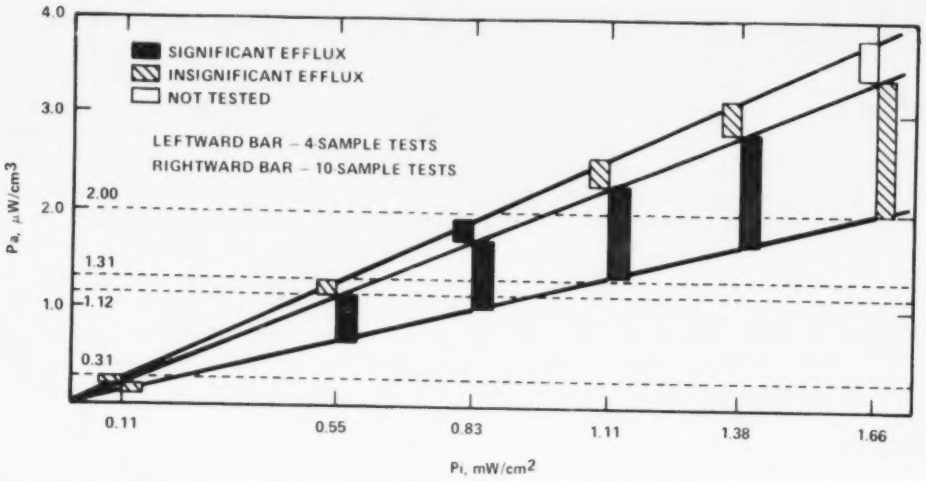

Fig. 5. Ranges of spatial variation of absorbed power density P_a within a spherical sample versus incident power density P_i for four-sample and ten-sample tests. Effective values of P_a may occur anywhere between the limits set by negative experiments (0.31–1.12 μW/cm^3 and 1.31–2.00 μW/cm^3).

corresponding change in P_a for this error in P_i would be barely noticeable in the bar heights of Fig. 5.

Conclusions

The results of the calcium-ion efflux work reported by Blackman *et al.* [2] showed the range of effective incident power densities for ten-sample exposures to be different from the effective range for four-sample exposures. These results can now be explained by taking the absorbed power density P_a within the sample to be the important variable governing the outcome of the experiments.

There are several ways to evaluate the data to determine the values of effective absorbed power density. One approach in identifying effective values of P_a is to use the results of negative experiments to define the limits within which enhanced efflux may occur. For example, referring to Fig. 5, we use the four-sample negative results at 0.11 and 0.55 mW/cm^2 and the ten-sample negative results at 1.66 mW/cm^2 as boundaries to define two broader ranges of potentially effective P_a values, from 0.31 to 1.12 μW/cm^3 and from 1.31 to 2.00 μW/cm^3. This approach assumes there may be one or more values of P_a within these two ranges that are effective in producing calcium efflux.

Hence, to explain the test results, there must be at least two power windows or ranges within which an effective value of P_a occurs. From the limits indicated above, the window widths may be 0.81 and 0.69 μW/cm^3 (as in Fig. 5). At this time, we do not have enough information to be more specific about the range of effective values of P_a. Additional experiments will be conducted to further delineate the width and location of the power windows.

It thus appears that measurable enhancement of calcium-ion efflux occurs only when a large enough volume or surface area of tissue is exposed to a given range of power densities. It is possible that other power densities of RF radiation can stimulate enhanced calcium-ion efflux, but that this response involves such a small volume or surface area of tissue that it is below the detection limit of the biochemical assay procedure.

References

[1] C. F. Blackman, J. A. Elder, C. M. Weil, S. G. Benane, D. C. Eichinger, and D. E. House, "Induction of calcium-ion efflux from brain tissue by radio frequency radiation: Effects of modulation frequency and field strength," *Radio Sci.*, vol. 14(6S), pp. 93–98, Dec. 1979.

[2] C. F. Blackman, S. G. Benane, J. A. Elder, D. E. House, J. A. Lampe, and J. M. Faulk, "Induction of calcium-ion efflux from brain tissue by radio frequency radiation: Effect of sample number and modulation frequency on the field-strength window," *Bioelectromagnetics*, vol. 1, pp. 35–43, 1980.

[3] R. J. Spiegel, "ELF coupling to spherical models of man and animals," *IEEE Trans. Biomed. Eng.*, vol. BME-23, pp. 387–391, Sept. 1976.

[4] J. C. Lin, A. W. Guy, and C. C. Johnson, "Power deposition in a spherical model of a man exposed to 1–20 MHz electromagnetic fields," *IEEE Tran. Microwave Theory Tech.*, vol. MTT-21, pp. 791–797, Dec. 1973.

[5] K. R. Foster, J. L. Schepps, R. D. Stoy, and H. P. Schwan, "Dielectric properties of brain tissue between 0.01 and 10 GHz," *Phys. Med. Biol.*, vol. 24, pp. 1177–1187, 1980.

[6] J. Van Bladel, *Electromagnetic Fields*. New York: McGraw-Hill, 1964, ch. 9, pp. 282–291.

[7] J. A. Stratton, *Electromagnetic Theory*. New York: McGraw-Hill, 1941, ch. 3, p. 204.

[8] M. A. Hollis, C. F. Blackman, C. M. Weil, J. W. Allis, and D. J. Schaefer, "A swept-frequency magnitude method for the dielectric characterization of chemical and biological systems," *IEEE Trans. Microwave Theory Tech.*, vol. MTT-28, pp. 791–801, 1980.

William T. Joines (M'61) was born in Granite Falls, NC, on November 20, 1931. He received the B.S.E.E. degree with high honors from North Carolina State University, Raleigh, in 1959, and the M.S. and Ph.D. degrees in electrical engineering from Duke University, Durham, NC, in 1961 and 1964, respectively.

From 1959 to 1966, he was a member of the Technical Staff at Bell Telephone Laboratories, Winston-Salem, NC, where he was engaged in research and development of microwave components and systems for military applications. He joined the faculty of Duke University in 1966, and is currently a Professor of Electrical Engineering, as well as working in the U.S. Environmental Protection

Agency. His research and teaching interests are in the area of electromagnetic wave interactions with materials. He has published numerous papers in this area.

Carl F. Blackman received the A.B. degree in physics from Colgate University, Hamilton, NY, in 1963, and the M.S. and Ph.D. degrees in biophysics from Pennsylvania State University, University Park, in 1967 and 1969, respectively.

Following two years of postdoctoral work in Gerontology at Brookhaven National Laboratory, he joined the Bureau of Radiological Health in October 1970. He was transferred to the U.S. Environmental Protection Agency when the agency was created in December 1970, and has since been conducting research on the biological effects of nonionizing electromagnetic radiation, examining both the mutagenic potential of microwaves in bacteria and radiation-induced changes in ion-association with brain tissue. He is currently working as a Biologist for the U.S. Environmental Protection Agency in Research Triangle Park, NC.

Dr. Blackman is a member of the Biophysical Society, the American Society for Photobiology, and the Bioelectromagnetics Society.

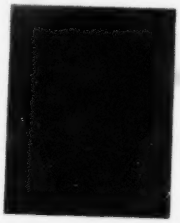

Mark A. Hollis (A'74-S'75) was born in Asheville, NC, on December 2, 1956. He received the B.S.E. degree in electrical engineering with distinction from Duke University, Durham, NC.

In his first 2 years at Duke, he was involved with maintenance, design, and development of campus audio and video systems. From January 1978 to August 1979 he was employed part time by the U.S. Environmental Protection Agency's Health Effects Research Laboratory in Research Triangle Park, NC. While there he was involved in the investigation of the biological effects of electromagnetic radiation. He is now in graduate study in Electrical Engineering at Cornell University, Ithaca, NY.

Mr. Hollis is a member of the Audio Engineering Society, Phi Eta Sigma, Eta Kappa Nu, Tau Beta Pi, and Phi Beta Kappa.